Journal of Hydrology 599 (2021) 126020

Contents lists available at ScienceDirect

Journal of Hydrology

journal homepage: www.elsevier.com/locate/jhydrol

Research papers

Reducing hydrological modelling uncertainty by using MODIS snow cover data and a topography-based distribution function snowmelt model

Nicola Di Marco [a], Diego Avesani [a], Maurizio Righetti [a,*], Mattia Zaramella [c], Bruno Majone [b], Marco Borga [c]

[a] Faculty of Science and Technology, University of Bozen/Bolzano, Bozen/Bolzano 39100, Italy
[b] Department of Civil, Mechanical and Environmental Engineering, University of Trento, Trento 38123, Italy
[c] Department of Land, Environment, Agriculture and Forestry, University of Padova, Legnaro (Padova) I-35020, Italy

ARTICLE INFO

This manuscript was handled by Emmanouil Anagnostou, Editor-in-Chief, with the assistance of Yang Hong, Associate Editor

Keywords:
Uncertainty analysis
MODIS snow cover maps
Multiobjective parameter estimation
Snow hydrology
Hydrological modelling

ABSTRACT

This work introduces a general multi-objective parameter estimation framework to exploit MODIS-based snow cover maps to reduce predictive streamflow uncertainty in snow-dominated catchments. The well-known GLUE methodology is applied with a multi-objective approach, combining streamflow observations recorded at the outlet section and satellite-derived snow cover maps, aggregated to fractional values of the catchment area. The hydrological model used in this study includes a snowpack routine which exploits a statistical representation of the distribution of clear sky potential solar radiation - a significant advantage when parameter sensitivity and uncertainty estimation procedures are carried out. The study provides an assessment of this approach based on operational quality data from two medium-size mountainous basins (a nested one included in a larger parent basin) located in the eastern Italian Alps. The nested basin is considered as ungauged, thus allowing a spatial assessment of the multi-objective approach. Results show a positive feedback between streamflow and snow cover area likelihoods, highlighted by means of the Pareto plot. Moreover, a better identifiability of the parameters driving snowmelt rate is found and consequently a shrink of the predictive streamflow uncertainty is observed. A containing ratio of 0.54 and a mean sharpness of 0.11 are found at the outlet of the parent basin, while a containing ratio equal to 0.65 and a mean sharpness equal to 0.17 are estimated at the nested basin, used as a validation test. These results confirm the potential of MODIS snow cover maps as additional data to inform hydrological models leading to more reliable and sharper streamflow simulations. This approach might be also appealing when streamflow simulations are required for ungauged basins.

1. Introduction

Hydrological models play a key role for supporting the development of efficient water resources planning, management and adaptation strategies. Indeed, they can provide valuable information to better address issues related to e.g. natural hazards such as floods and droughts, (Sene, 2010), competing water uses (Bellin et al., 2016) and hydropower energy production (Majone et al., 2016; Wagner et al., 2017). In snow-dominated catchments hydrological modelling reliability also depends on the capability of simulating snow accumulation and melting (Valéry et al., 2014; Warscher et al., 2013), since snow dynamics strongly affects floods (Förster et al., 2014) as well as both seasonal and annual runoff regimes (Mazouz et al., 2012).

Moreover, hydrological models output usually depends on several parameters. Accurate parameter estimation might be challenging because of the well-known equifinality issue (Beven, 2006), turning into potentially unreliable parameter estimates out of the model calibration period. Starting with the pioneering works of Duan et al., (1992) and Gupta et al., (1998) it was clear the need to consider the inherent multi-objective nature of the inference problem to quantify and reduce the uncertainty related to model parameter estimation. Several methods address the issue of multi-objective parameter estimation, as thoroughly described by Madsen (2003). Among the different approaches, multi-variable methods revealed their utility in improving parameter identifiability and model prediction capabilities (see Efstratiadis and Koutsoyiannis, 2010).

The main benefit of the multi-objective approach is an improved identification of the hydrological model, which in principle allows a

* Corresponding author.
E-mail address: maurizio.righetti@unibz.it (M. Righetti).

https://doi.org/10.1016/j.jhydrol.2021.126020
Received 22 August 2020; Received in revised form 21 December 2020; Accepted 18 January 2021
Available online 29 January 2021

good reproduction of the variable of interest (typically streamflow) without introducing large biases in the simulation of the other components of the hydrological cycle (Wagener et al., 2001). Such methodology proved to be effective also in snow-dominated catchments, where streamflow records and snow-related observations (e.g. ground or satellite data) are used simultaneously. Snow-related observations have been typically used for improving the performances of hydrological models through calibration experiments (see e.g. Tuo et al., 2018; Shrestha et al., 2014; Roy et al., 2010; Parajka and Blöschl, 2008b). Among the different types of snow-related measurements, satellite-derived snow cover data have been increasingly used to improve runoff estimates (Parajka and Blöschl, 2008b; Parajka et al., 2012; Shrestha et al., 2014; Riboust et al., 2019) as well as joint streamflow and snow water equivalent predictions (Stigter et al., 2017). In this context, the Moderate resolution Imaging Spectroradiometer (hereinafter referred as MODIS) snow cover maps represent a valuable information due to their high temporal (i.e. 1 day) and spatial resolution (i.e. 500 m, according to the standard NASA products). MODIS snow cover area (SCA) maps accuracy was extensively validated across different areas by comparison with in-situ snow depth observations (Parajka and Bloschl, 2006; Notarnicola et al., 2013b; Di Marco et al., 2020) and other satellite-derived snow cover products, such as LANDSAT (Gascoin et al., 2015).

MODIS-based SCA and streamflow records were used jointly by Teweldebrhan et al., (2018) to perform uncertainty parameter estimation of a conceptual hydrological model. However, despite a better parameter identifiability the authors did not find any significant improvement in streamflow simulation. Other studies focused on the joint application of streamflow data and MODIS-based SCA retrievals, though hydrological response uncertainty quantification combining such datasets did not receive adequate attention in the literature, as reported by Teweldebrhan et al., (2018). Finger et al., (2015) used streamflow data, MODIS SCA and glacier mass balance records to improve the robustness of HBV model estimating model parameters within a Montecarlo framework. Shrestha et al. (2014) combined MODIS SCA maps with streamflow to improve the spatial distribution of snowfall in a small size catchment and in turn the accuracy of the simulated streamflow. A similar approach, based on AVHRR (Advanced Very High Resolution Radiometer) retrievals, was presented by Duethmann et al. (2014) to evaluate the benefit of using an increasing number of images within a multi-objective model parameter estimation framework. However, none of the abovementioned studies focused on the explicit quantification of predicted streamflow uncertainty reduction or on the validation of the proposed modelling at nested sites within the catchments, i.e. a spatial validation of the parameter estimation procedure. We speculate that the scarce literature on combining satellite-derived SCA and streamflow data within an uncertainty framework might be caused by the large computational effort of such analysis. Indeed, reproducing a massive number of model realizations for the variables of interest, e.g. streamflow, Snow Water Equivalent (SWE) and SCA, as required for a thorough uncertainty estimation analysis, might be very expensive from a computational point of view. This is especially true for spatially distributed variables, such as SWE which in turn leads to the SCA quantification. In this work, we exploited the capabilities of TOPMELT (Zaramella et al., 2019), a recently proposed extended temperature index model particularly suited for Montecarlo-based uncertainty analyses, as shown by Di Marco et al. (2020) comparing TOPMELT and MODIS-based SCA over an Alpine catchment.

Based on the abovementioned background, we aim to introduce a general multi-objective parameter estimation framework to exploit MODIS-based SCA maps to reduce predictive streamflow uncertainty in snow-dominated catchments. Such framework is relatively easy to extend over different, even data-scarce, regions. We also provide a spatial validation of the proposed framework simulating streamflow in a nested sub-catchment, where streamflow data are available but not used in the parameter estimation phase. Finally, we show how MODIS-based SCA information might be used to reduce SWE predicted uncertainty, even though it is acknowledged that a validation is not provided because of lack of data.

The paper is organized as follows: Sect. 2 provides a short description of the adopted hydrological and snowpack models, the case study area and the multi-objective parameter estimation method. Main results are presented in Sect. 3, and further discussed in Sect. 4. Finally, Sect. 5 reports some concluding remarks.

2. Materials and methods

2.1. Hydrological and snowpack model

The conceptual, semi-distributed hydrological model ICHYMOD (Norbiato et al., 2009; 2008) was used to simulate hydrological fluxes at hourly time resolution. ICHYMOD exploits the runoff production module of the PDM rainfall-runoff model (Moore, 2007; 1985), in which the so-called probability distributed soil moisture storage, a function that describes the spatial variability of the soil infiltration capacity, is used to estimate the rainfall excess. The PDM takes up water from rainfall and snowmelt and loses water by evapotranspiration and recharge to groundwater, computed as a function of the soil water content through a power law relationship. Potential evapotranspiration is estimated by means of the Hargreaves model. Direct runoff is routed to the outlet of the sub-basin by means of a cascade of two linear reservoirs, while baseflow is transferred downstream through the adoption of a nonlinear storage. The well-known Muskingam-Cunge scheme is used to propagate the flow from each sub-basin outlet along the river network.

The required meteorological inputs are hourly time series of precipitation and temperature. Snow accumulation and melting are computed by means of TOPMELT (Zaramella et al., 2019; Puspitarini et al., 2020; Scorpio et al., 2020) model. TOPMELT is a semi-distributed snowpack model based on an extended temperature index approach capable to estimate the full spatial distribution of the SWE at each time step. The clear sky shortwave solar radiation is computed at each element of the digital terrain model (DTM) by taking into account shadow and complex topography, calculating the apparent sun motion and the intersection of radiation with topography. Diffuse radiation is computed by accounting for self-shading (by slope and aspect) and occlusions produced by the visible horizon. With TOPMELT, the catchment is divided into elevation bands and the full spatial distribution of clear sky potential solar radiation is discretised into a number of radiation classes for each elevation band. The computation required to generate a spatially distributed water equivalent thus reduces to a single calculation for each radiation class, ensuring a high computational efficiency. The work by Zaramella et al. (2019) shows that aggregating radiation into ten classes for each elevation band has a minimal impact on model results, compared to a distributed model. Therefore, based on the spatial distribution of the clear sky solar radiation, pixels included in each elevation band are grouped in ten radiation classes. The snowmelt routine is applied to each radiation class in place of to each pixel.

During day dry hours, the snowmelt rate $F_{i,j}(t)$ [mm·h^{-1}] for the *i-th* elevation band, the *j-th* radiation class and at time t is computed as follows:

$$F_{i,j}(t) = CMF \cdot RI_{i,j}(t) \cdot (1 - alb_s(t)) \cdot max\{0; T_i(t) - T_b\} \quad (1)$$

where CMF is the combined melting factor [mm·m^2 ·$^\circ$C^{-1}·MJ^{-1}], RI is the clear sky solar radiation [MJ·m^{-2}·h^{-1}] and $alb_s(t)$ is the snow albedo [-] at the current time step t, modelled as a function of the fresh snow albedo, alb_s (Brock et al., 2000). T_i is the air temperature at the *i-th* elevation band while T_b is the temperature threshold above which snowmelt is assumed to occur, both in [°C]. The model accounts for rain-on–snow and melt during night by means of a temperature index approach, through two additional parameters, the rain melt factor (RMF) and the night melt factor (NMF) respectively (see Zaramella et al. 2019 for further details).

With TOPMELT, air temperature is computed at each elevation band by assuming a linear temperature lapse rate, estimated at hourly time step with a linear regression on the available temperature data. To account for gauge catch deficiencies that occur during periods of snow, precipitation data are corrected with a snow correction factor (*SCF*). *SCF* is set to the constant value of 1.4 after a sensitivity analysis and in agreement with previous works conducted over the Upper Adige river basin (Engel et al., 2017; Di Marco et al., 2020). For the analyses reported in this work, the Thiessen method was used to calculate the mean precipitation over the basin. Then, the mean areal precipitation estimate was corrected with a Precipitation Correction Factor (*PCF*) to account for poor spatial representativeness of the rain gages. *PCF* is a dimensionless parameter acting as a multiplicative factor on the mean sub-catchment precipitation. Moreover, a lapse rate (*G*) is applied to distribute such mean areal precipitation over each elevation band. Estimation of the precipitation phase (solid or liquid) is therefore performed over each elevation band, according to the threshold temperature T_c.

The selection of the parameters involved in the uncertainty analysis (among all those available in the PDM implementation, see Moore, (2007)), was performed on the basis of a preliminary sensitivity analysis conducted with the GLUE method (Beven and Binley, 1992). The list of the ten PDM-TOPMELT calibration parameters adopted in the present study is presented in Table 1 together with their respective ranges of variation.

2.2. Study area and data

The analysis was performed over the Passer/Passirio river basin (428 km^2), one of the main tributaries of the Adige river basin, Eastern Italian Alps (Fig. 1) (Stergiadi et al., 2020), with elevations ranging between 360 m a.m.s.l. and 3500 m a.m.s.l.. Two basins in the Passer/Passirio river system were considered: Passer/Passirio river basin at Meran (414 km^2) and its sub-basin Plan river at Pfelders/Plan (49 km^2). Precipitation and temperature data from nine weather stations (Table 2) as well as discharge data at the two outlet sections are available at hourly time step over the period selected for the study, ranging from 01/10/2014 to 30/09/2017. The mean annual precipitation over the Passer/Passirio river basin in the period of interest is about 1150 mm, close to the long term annual average (Chiogna et al., 2016; Mallucci et al., 2019; Avesani et al., 2021). Precipitation mainly occurs in fall and summer (Fig. 2a), as typically observed across the Adige river basin (Laiti et al., 2018; Chiogna et al., 2016). Fig. 2b and Fig. 2c show the monthly pattern of the hourly unit discharge at Meran/Merano and Pfelders/Plan, respectively. The hydrological regime is a typical snow-dominated regime, with a significant difference between winter low-flows and spring high-flows.

Table 1
List of model parameters for snow and rainfall-runoff modules (respectively TOPMELT and PDM models) and their respective ranges of variation.

Parameter	Unit	Range	Description	Sub-Model
PCF	–	1 – 1.2	Precipitation correction factor	TOPMELT
CMF	mm m^2 MJ^{-1} °C^{-1}	0.001 – 0.1	Combined melt factor	TOPMELT
G	% mm km^{-1}	0 – 0.5	Precipitation gradient with altitudes	TOPMELT
alb_s	–	0.70 – 0.95	Fresh snow albedo	TOPMELT
T_c	°C	0 – 2.5	Threshold temperature for rain/snow classification	TOPMELT
RMF	mm h^{-1} °C^{-1}	0.05 – 0.90	Rain melt factor	TOPMELT
C_{max}	mm	100 – 500	Maximum storage capacity	PDM
b	–	0.025 – 0.75	Exponent of storage capacity probability distribution function	PDM
K_g	hh mm^{bg-1}	20,000 – 60,000	Groundwater recharge time constant	PDM
b_g	–	1.3 – 2.3	Exponent of groundwater recharge function	PDM

The hydrological model was applied to the Passer/Passirio watershed by dividing the main basin in different sub-catchments (average size about 20 km^2) over which hydrological properties are assumed to be uniform. Flow data from the Plan river basin at Pfelders/Plan were used to validate the robustness of our analysis at a location different from that selected during the model conditioning procedure. Accordingly, the streamflow records of Pfelders/Plan station were not involved in the parameter identification phase.

Daily snow cover area maps were provided with a spatial resolution of 250x250m by EURAC (Notarnicola et al., 2013a; 2013b). This resolution is finer than the standard NASA MODIS snow products (500x500m) and allows better snow detection at a local scale especially in harsh environments (Notarnicola et al., 2013a), where topography and land cover (i.e. forests) may prevent an optimal signal acquisition by MODIS (Simic et al., 2004; Engel et al., 2017). Moreover, EURAC products have been extensively tested in other studies conducted either in the Eastern Italian Alps (Engel et al., 2017; Di Marco et al., 2020) and across Europe (Thirel et al., 2012).

MODIS SCA maps were processed to discard days with cloud coverage greater than a fixed fraction of the catchment area. Following Finger et al., 2015 we fixed this threshold value at 10% of the total Passer/Passirio catchment area, i.e., about 41 km^2. Moreover, we discarded MODIS maps during the period from July to September since fractional SCA was negligible and limited to high elevation portions of the watershed, where MODIS products is known to be less reliable mainly because of cloud misclassifications and patchy snow covered area (Parajka and Blöschl, 2008a; Notarnicola et al., 2013b).

As a result, a discontinuous time series of 187 days of snow cover area maps was made available as an input for the multi-objective parameter estimation method (see Sect. 2). Following Duethmann et al. (2014), we assumed that the presence of gaps in the data did not affect the multi-objective uncertainty analysis procedure.

A good consistency between TOPMELT outputs and MODIS-based SCA was found by Di Marco et al. (2020) either in terms of fractional snow covered area, *fSCA* (i.e. the percentage of the overall catchment area covered by snow, based on either MODIS maps or simulated spatial distributions of snowpack) and SCA spatial distribution carried out on a sub-catchment of the upper Adige river basin, which includes the Passer/Passirio tributary area. Following that work, we estimated TOPMELT *fSCA* taking advantage of the distributed structure of the snowpack model, which allows to estimate the fractional snow covered area as the ratio between the area with SWE greater than a fixed threshold and the total area of the catchment. Such threshold was set equal to 5 mm SWE. Moreover, it has to be specified that TOPMELT works at hourly time step, while MODIS maps are available on a daily basis. Therefore, daily time series of TOPMELT *fSCA* were estimated, averaging the original hourly simulations.

2.3. Uncertainty estimation methodology

2.3.1. Selection of behavioural simulations with the GLUE approach

Model parameters uncertainty estimation was performed using the Generalized Likelihood Uncertainty Estimation, i.e. the GLUE methodology (Beven, 2006). GLUE relies on the generation of a high number of independent model realizations (i.e., Monte Carlo simulations), each associated with a specific parametrization and a likelihood measure. The selection of both the likelihood measure and the cutoff threshold separating behavioral from non-behavioral simulations is a subjective choice of the modeler (Blasone et al., 2008; Jin et al., 2010). Furthermore, the procedure is not meant to find a single optimum configuration, yet a set

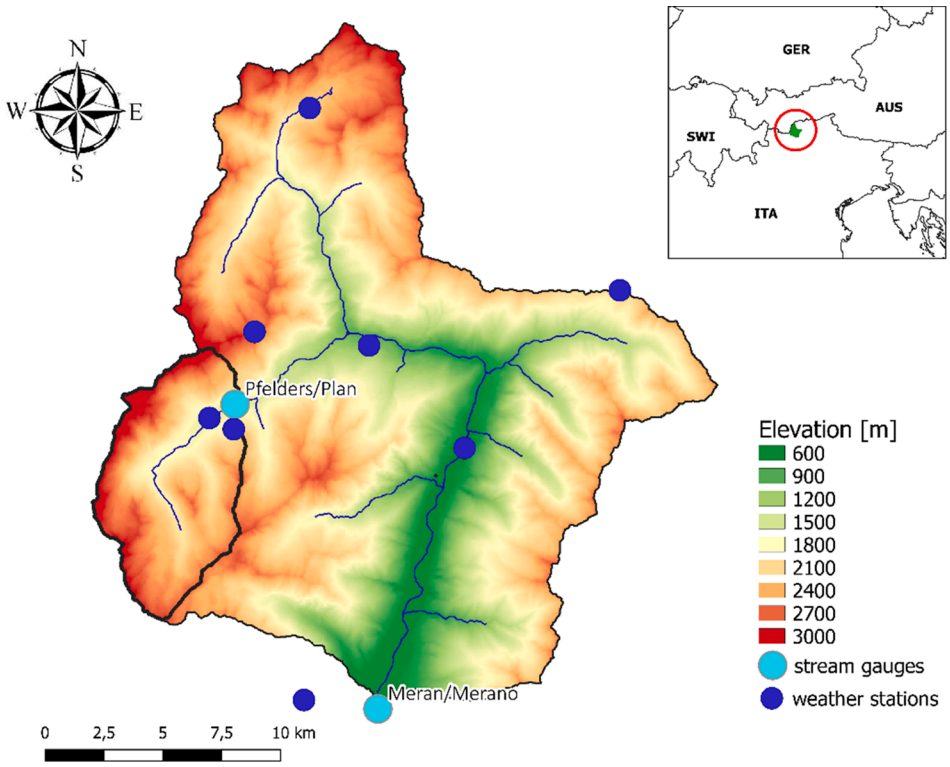

Fig. 1. Map showing the Passer/Passirio river basin closed at Meran/Merano station (414 km^2), the Pfelders/Plan nested sub-basin (49 km^2), the digital elevation model, the main stream network and the locations of available weather stations and stream gauges.

Table 2
List of available weather gauging stations including the percentage of available measurements of temperature and precipitation.

Station	Elevation [m]	Time fraction of available temperature data [%]	Time fraction of available precipitation data [%]
Meran/Merano (APPA)	297	94	77
Meran/Merano	333	100	100
Sankt Martin/San Martino	586	100	100
Platt/Plata	1147	94	92
Pfelders/Plan	1618	99	99
Prati di Pfelders/ Plan	2015	96	–
Jaufenkamm/ Giovo	2145	100	–
Timmelsalm/Alpe del Tumulo	2230	46	58
Pfelders Rauhjoch/ Monte Scabro	2926	100	–

of acceptable models (Efstratiadis and Koutsoyiannis, 2010; Brazier et al., 2000), according with the abovementioned concept of equifinality.

Accordingly, first of all we performed a random sampling from the parameter space by means of Latin Hypercube Sampling scheme (McKay et al., 1979), assuming a uniform distribution for every parameter listed in Table 1. Since we did not have any a-priori information about the parameter distribution, we considered each parameter set as equally likely (see e.g., Gan et al., 2018; Teweldebrhan et al., 2018). To this end, a sample of 10,000 different parameter sets was generated, each associated with a likelihood measure for the evaluation of the modelling efficiency. Behavioural parametrizations were then identified based on

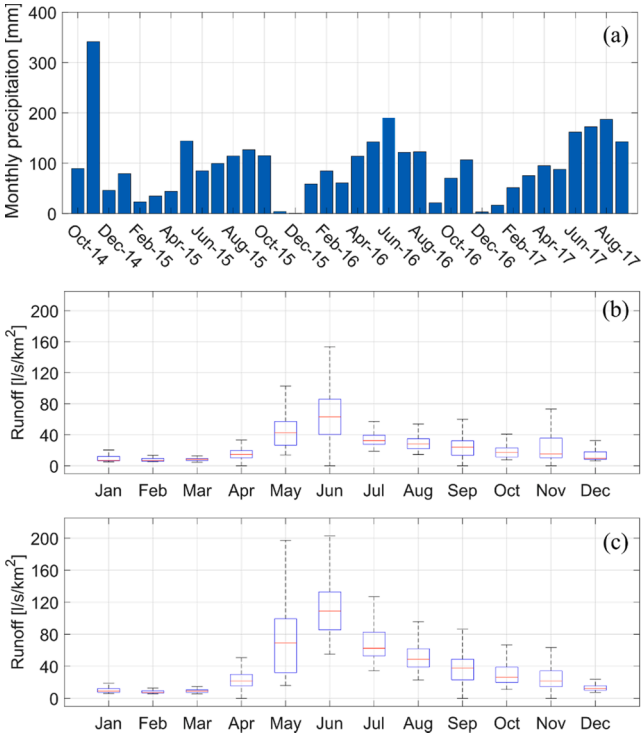

Fig. 2. Total monthly mean areal precipitation for the Passer/Passirio river basin closed at Meran/Merano (a), monthly distribution of the specific hourly discharge measured at Meran/Merano (b) and at Pfelders/Plan (c) river sections. The whiskers show the minimum and maximum values while the box width is the interquartile range. The period considered ranges from 01/10/2014 to 30/09/2017.

suitable thresholds. Simulations producing likelihood measures below the identified thresholds were considered not behavioural and their likelihoods were set equal to 0. The likelihoods associated with the retained simulations (i.e., behavioral parameter set) were rescaled so that their cumulative total is one, with the resulting probability density function representing our new knowledge about the model parameters. Moreover, in order to estimate the predictive uncertainty bounds of the simulated variables (e.g. streamflow), the behavioural runs were ranked according to the magnitude of the rescaled likelihood measure producing the empirical cumulative likelihood weighted distribution (Efstratiadis and Koutsoyiannis, 2010; Brazier et al., 2000; Franks et al., 1998). The uncertainty range is given by such cumulative distribution, neglecting the tails identified with the quantiles 5% and 95% (Teweldebrhan et al., 2018).

As likelihood measure for both streamflow and *fSCA* variables we used the Nash-Sutcliffe efficiency (NSE, Nash and Sutcliffe, 1970) index. The streamflow NSE is computed as follows:

$$NSE(Q) = 1 - \frac{\sum_{t=1}^{N}(Q_{sim}(t) - Q_{obs}(t))^2}{\sum_{t=1}^{N}(Q_{obs}(t) - Q_{obs,mean})^2} \quad (2)$$

while the fractional SCA NSE assumes the following form:

$$NSE(fSCA) = 1 - \frac{\sum_{t=1}^{N}(fSCA_{sim}(t) - fSCA_{MODIS}(t))^2}{\sum_{t=1}^{N}(fSCA_{MODIS}(t) - fSCA_{MODIS,mean})^2} \quad (3)$$

where t is the current time step, Q_{sim} and Q_{obs} are the simulated and observed streamflow time series, respectively, $Q_{obs,mean}$ is the mean observed streamflow, $fSCA_{sim}$, and $fSCA_{obs}$ are the simulated and MODIS-based fractional snow covered area time series, respectively, and $fSCA_{MODIS,mean}$ is the MODIS-based averaged fractional snow covered area. Finally, N is the total number of time steps.

Following Moriasi et al., 2007, the threshold for the identification of behavioural streamflow simulations was set at 0.5. The selection of the threshold value for NSE(*fSCA*) deserves an in depth discussion that is provided in Sect. 4.1; here it is worth noting that the value was fixed equal to the median of the simulated NSE(*fSCA*) values, resulting in a NSE(*fSCA*) = 0.67.

2.3.2. Multi-objective parameters estimation

Multi-objective parameters estimation was carried out in two separate steps following an informal Bayesian approach. First, streamflow measurements recorded at Meran/Merano hydrometric gauging station (i.e. the catchment outlet section) were used to constrain model parameters. The resulting distribution of the likelihood measures was assumed as informative of the prior information, i.e., it defines our knowledge about the system before introducing the additional MODIS *fSCA* data. Next, the combined (posterior) likelihood distribution (*cLH*) was estimated multiplying streamflow and *fSCA* likelihoods (eqn. (2) and (3)) and introducing a suitable rescaling factor C in order to obtain a combined probability distribution function (see e.g., Brazier et al., 2000; Franks et al., 1998, among others). This function represents the posterior parameter distribution:

$$cLH(p_i|Q, SCA) = \frac{1}{C} \cdot LH(Q|p_i) \cdot LH(fSCA|p_i) \quad (4)$$

where p_i is one of the parameter sets considered in the Monte Carlo sample sampling, $LH(Q|p_i)$ is the streamflow likelihood (i.e. the prior distribution), $LH(fSCA|p_i)$ is the snow cover-related likelihood obtained by comparing TOPMELT module outputs and MODIS fractional SCA data. Finally, C is a normalization constant introduced in order to have a unitary integral of $cLH(i)$. Observed streamflow time series available at the Pfelders/Plan gauging station were used only for the spatial validation of our approach and hence were not considered for model conditioning.

2.4. Metrics for uncertainty quantification

We used two metrics to quantify the benefit of multi-objective model conditioning over the mono-criteria case (i.e. the case in which only streamflow observations are exploited). The first metric is the so-called containing ratio *CR*, (Teweldebrhan et al., 2018), also known as reliability (Zhang et al., 2008), defined as following:

$$CR = \frac{1}{N} \cdot \sum_{t=1}^{N} I(O(t); X_{sim0.05}(t); X_{sim0.95}(t)) \quad (5)$$

where t is the current time step, N is the total number of time steps and $O(t)$, $X_{sim\ 0.05}(t)$ and $X_{sim\ 0.95}(t)$ are respectively the observed variable (i.e. streamflow or *fSCA*) and the prediction corresponding to the 0.05 and 0.95 percentiles. I is a function that assumes the values of 1 if the simulated percentile range brackets the observation, and 0 otherwise.

The second metric we adopted is the sharpness (Shafii et al., 2014; Zhang et al., 2008), which allows to estimate the reduction of the prediction uncertainty range obtained by adding MODIS *fSCA* data in the parameter constraining process. Sharpness (*SH*) is defined as 1 minus the ratio between the posterior uncertainty range of a given variable to the uncertainty range given by the prior distribution, as reported in eqn. (6).

$$SH = 1 - \frac{cLH(p_i|Q, fSCA)}{LH(Q|p_i)} \quad (6)$$

Notice that a perfect model conditioning would lead to both *CR* and *SH* equal to 1, assuming a predicted posterior uncertainty range that asymptotically tends to 0. In other words, with a perfect multi-objective conditioning the predicted uncertainty band tends to 0, i.e. the simulated variable has no uncertainty. Accordingly, such simulated variable would perfectly match the observation, thus leading to *CR* equal to 1.

3. Results

As specified in Section 2, the parameters of the hydrological model were inferred by maximizing the likelihood measures at Meran/Merano gauging station during the period from 01/10/2013 to 30/09/2017. The first year of the time series, 01/10/2013–30/09/2014, was used as spin-up period for the simulations and therefore was excluded from the computation of the efficiency metrics within the GLUE procedure.

Model parameters were conditioned using only streamflow records at the catchment outlet (Meran/Merano station) to identify a-priori information, then we applied the multi-objective conditioning to infer posterior parameter distributions combining both streamflow observations at Meran/Merano and fractional SCA data relative to the overall catchment area. Finally, prediction uncertainty of streamflow, *fSCA* and mean areal Snow Water Equivalent (SWE) were estimated either at Meran/Merano and at Pfelders/Plan basins using both prior and poster parameter distributions. Such approach allows to quantify to what extent the parametric uncertainty might be reduced because of the joint use of *fSCA* and streamflow information. We highlight that we consider the Pfelders/Plan catchment as ungauged, therefore it can be considered as a validation test for the proposed approach.

3.1. Behavioral simulations

For each run of the overall Monte Carlo sample, we computed likelihood values for both streamflow and *fSCA*, using streamflow records taken at Meran/Merano stream gage and MODIS *fSCA* relative to the overall Passer/Passirio catchment. The Pareto fronts (green dots in Fig. 3) obtained either at Meran/Merano and Pfelders/Plan locations are presented in Fig. 3, together with the entire set of dominated solutions (i.e. solutions not belonging to the Pareto front). We remark again that *fSCA* observations were not used for the identification of behavioural

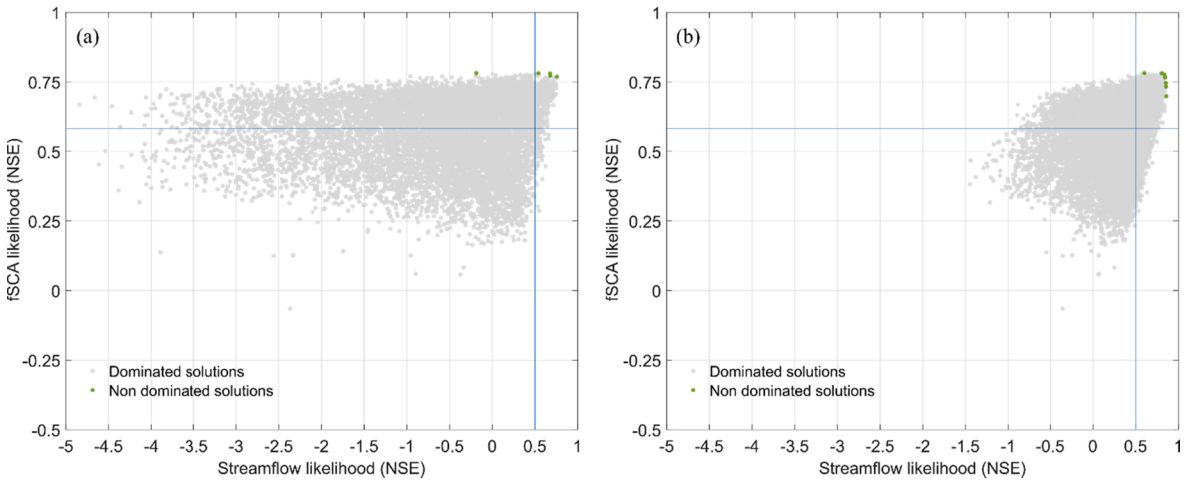

Fig. 3. Pareto fronts (green dots) of streamflow and *fSCA* likelihoods for (a) Meran/Merano and (b) Pfelders/Plan hydrometric gauging station, respectively. The thin blue lines represent the NSE thresholds defined for the multi-objective behavioural selection: NSE(Q) = 0.5 and NSE(*fSCA*) = median value, where *fSCA* is evaluated on the overall catchment. The dominated space of solutions is also shown as grey dots, i.e. the solutions for which a better solution in terms of either streamflow or fSCA exists. (For interpretation of the references to colour in this figure legend, the reader is referred to the web version of this article.)

simulation (i.e., a priori information) but only for ensuing identification of posterior parameter distributions.

Fig. 3 highlights that for both sites a positive feedback between *fSCA* and streamflow likelihoods is present. In other words, an increase of streamflow likelihood is not associated with a decrease of likelihood values for *fSCA*, as often observed in multi-objective optimization problems (Yapo et al., 1998). Such positive feedback is even more evident at Pfelders/Plan location, where snow dynamics controls the hydrological regime more largely than at Meran/Merano because of higher elevation and smaller drainage basin size.

3.2. Prior and posterior parameter distributions

Prior (i.e., model conditioning conducted using only Meran/Merano streamflow data) and posterior distributions for each model parameter are shown in Fig. 4. It is worth noting that in the figure we report only the comparison for TOPMELT module parameters, since the parameter distributions relative to the rainfall-runoff module did not show any appreciable variation. This result is expected since multi-objective model conditioning is performed using *fSCA* as additional data, therefore it seems reasonable that the further constrain on model parameters acts only in snow-related parameters.

Visual inspection of prior parameter distributions (blue lines in Fig. 4) evidences that Combined Melting Factor (*CMF*) and Precipitation Correction Factor (*PCF*) are the most sensitive parameters, i.e. their likelihood distributions vary significantly depending on the parameter value. Both parameters are related with the streamflow generation in a straightforward manner since snowmelt is linearly dependent to *CMF* through Eq. (1) and *PCF* is a multiplier of the estimated precipitation values introduced in order to compensate poor spatial representativeness of rain gages. Not surprisingly, for *PCF* values far from 1 the likelihood shows a sharp decrease, suggesting that precipitation estimates requires only a slight adjustment in this case study. We double-checked the reliability of available meteorological data estimating the runoff

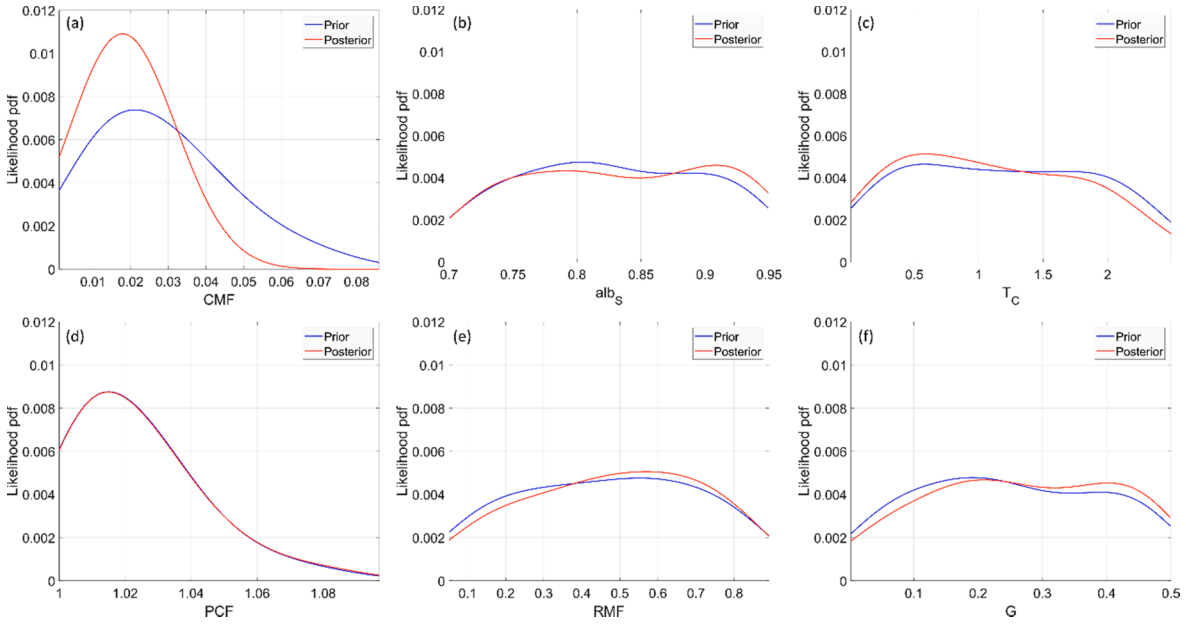

Fig. 4. Snow-related parameter distributions obtained by conditioning the model with streamflow observations recorded at the Meran/Merano station (prior pdf) and by combining streamflow measures with fractional MODIS-based snow-covered area (posterior pdf).

coefficient (i.e. the ratio of the total annual runoff over the total annual precipitation) for several hydrological years and the analysis confirmed that *PCF* optimal value is coherently close to 1. Posterior parameters distribution for alb_s, T_c, *RMF* and *G* display an almost flat behaviour for most of their range of variation and start to decrease significantly toward the boundaries of the range. This means that the interplay among the parameters has a major role in determining the likelihood rather than the variation of the single parameter (Beven and Freer, 2001).

The multi-objective model conditioning based on *fSCA* data has a different impact on the parameter distributions depending on the considered parameter. *CMF* is the parameter mostly affected by the further constrain imposed by *fSCA* data (Fig. 4a). Concerning the other posterior parameter distributions shown in Fig. 4, the effect of using MODIS *fSCA* as additional data is not as clear as *CMF*. *PCF* posterior distribution (Fig. 4d) almost does not show any differences with respect to the prior distribution, while a slight better parameter identifiability is observed for the parameters alb_s, T_c, *RMF* and *G* (Fig. 4b, Fig. 4c, Fig. 4e, Fig. 4f).

3.3. Streamflow and fSCA prediction uncertainty range

The prior and posterior likelihood-weighted cumulative distributions estimated as described in Sect. 2 are here used to simulate the 5–95% percentile prediction uncertainty range for both hourly streamflow and

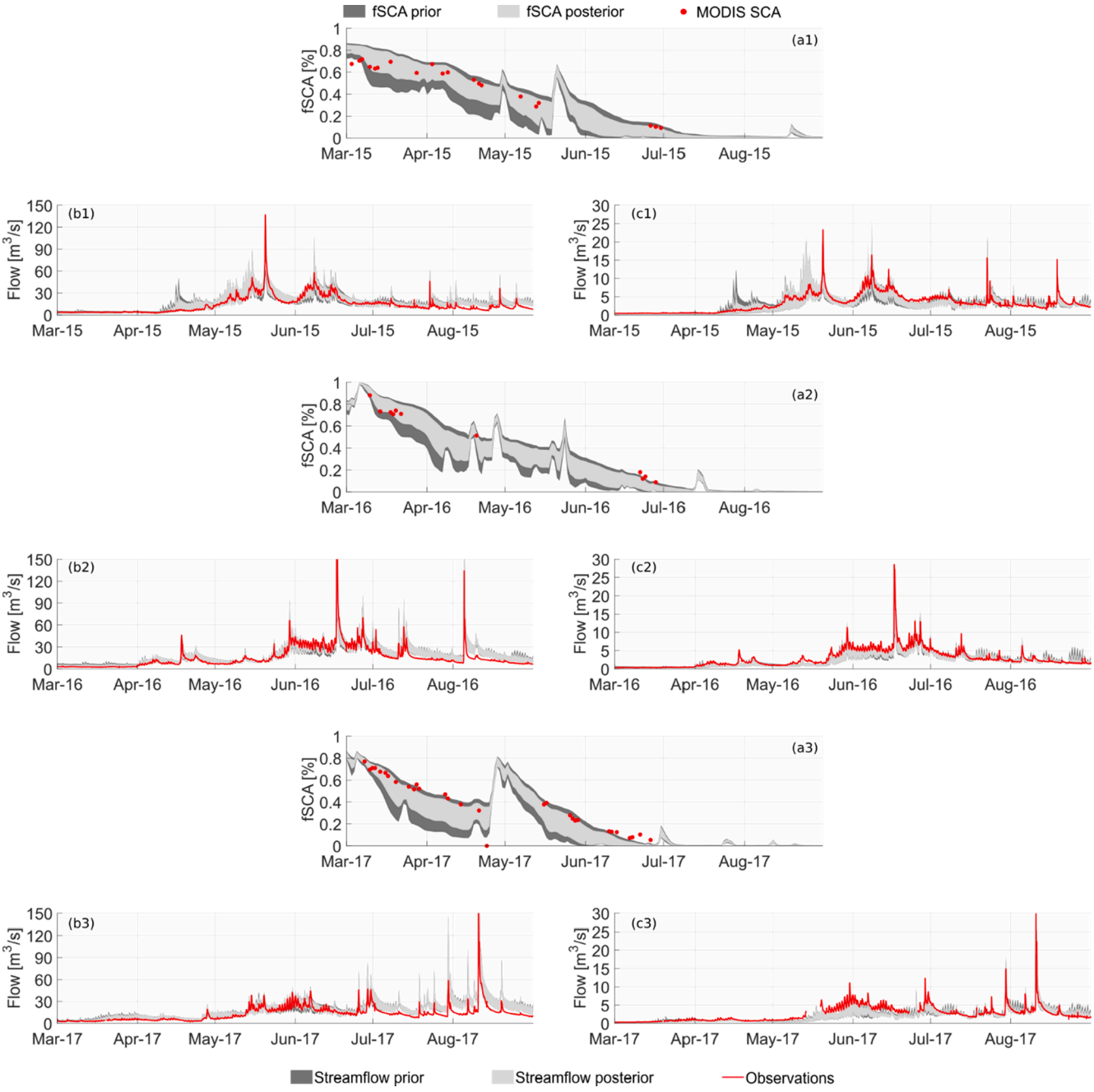

Fig. 5. 5–95% percentile prior and posterior predictive uncertainty ranges for fSCA (a1), streamflow at Meran/Merano station (b1) and streamflow at Pfelders/Plan station (c1) for the sub-period 2015/03/01–2015/08/30. The same variables are also shown for the following sub-periods: fSCA (a2), Meran/Merano streamflow (b2) and Pfelders/Plan streamflow (c2) for 2016/03/01–2016/08/30; fSCA (a3), Meran/Merano streamflow (b3) and Pfelders/Plan streamflow (c3) for 2017/03/01–2017/08/30. MODIS-based fSCA (red dots) and observed streamflow time series at Meran/Merano and Pfelders/Plan (red lines) are also presented. (For interpretation of the references to colour in this figure legend, the reader is referred to the web version of this article.)

daily *fSCA*. We remind that prior distribution was obtained by conditioning the model using only Meran/Merano streamflow data, while posterior distributions was derived from multi-objective conditioning using MODIS *fSCA* data over the same basin. The comparison between available observations and predictive uncertainty ranges is summarised in Fig. 5, where for easiness of visualization the overall time window is split into three sub-periods ranging from March 01 to August 31 for 2015, 2016 and 2017 years. We concentrated our attention on the period from March to August of every year since snowmelt occur mostly in these months, as confirmed by the observed *fSCA* time series (Fig. 5a1-3), which range from about 0.8 at beginning of March to about 0.05 at the beginning of August, for every year. Dark grey bands in Fig. 5a1-3 represent the predictive uncertainty range related to the prior distribution, meaning that the hydrological modelling (including simulation of *fSCA*) was conditioned only based on observed streamflow data at the Meran/Merano gauging station. The predictive uncertainty range includes most of the available MODIS-related *fSCA* observations, which we remind are not available continuously in time due to cloud cover issues (see Sect. 2). The uncertainty range of *fSCA* derived from prior information is relatively large, up to 0.5 during the spring snowmelt season (e.g. April 2016). As expected, the multi-objective conditioning leads to a narrower predictive uncertainty range (light grey band) over the entire melting season, particularly from March to May, i.e. during the onset of the snowmelt season. At the end of the melting season the simulated predictive uncertainty range, regardless if estimated using prior or posterior distributions, tends to slightly underestimate MODIS-based *fSCA* across the different years, especially on 2017, the driest year of the considered sample.

Streamflow predictive uncertainty ranges are shown in Fig. 5b1-3 and Fig. 5c1-3 for Meran/Merano and Pfelders/Plan gauging stations, respectively. Similarly to the case of *fSCA* both prior (dark grey) and posterior (light grey) uncertainty ranges are presented. In general, higher streamflow values are associated with larger uncertainty ranges due to the interaction among the different perturbed rainfall-runoff and snow related parameters. Visual inspection reveals that the larger shrink of the predictive uncertainty bounds occurs during the spring/summer 2015, while during years 2016 and 2017 the difference between prior and posterior distribution is less evident and mostly occurring on June. We attribute this to the presence of a very wet winter season in 2014/2015 (Fig. 2a) that leads to a persisting snowmelt control on the hydrological regime over spring and summer 2015. Accordingly, average *SH* values reported in Table 4 highlight the ability of multi-objective conditioning in reducing the predictive uncertainty band at both locations. In particular, streamflow mean *SH* estimated at Meran/Merano hydrometric station is 0.11 while at Pfelders/Plan is 0.17. A more detailed discussion on this is provided in Section 4. Fig. 6 shows the temporal evolution of *SH* time series at both gauging stations. In general, *SH* is positive (i.e. posterior uncertainty range is narrower than prior one), but some periods display a sharpness lower than 0, meaning that in such periods the multi-objective failed in improving the sharpness of the prediction.

The reliability of the predictive streamflow uncertainty range was assessed through the containing ratio index (Table 5). *CR* relative to prior distribution is 0.54 at Meran/Merano and 0.73 at Pfelders/Plan. Considering the case in which MODIS-related SCA data are used (posterior distribution) *CR* is still 0.54 at Meran/Merano while slightly decreases to the value of 0.65 at Pfelders/Plan. Moreover, we estimated the containing ratio focusing only on the sub-periods with positive sharpness. This aims to assess that the narrower uncertainty band of the posterior streamflow distribution does not lead to a failure in reliability. *CR* at Meran/Merano is 0.46, resulting in a reduction of about 10% compared with the posterior *CR* estimated throughout the simulated period. At Pfelders/Plan site *CR* is 0.59, showing a reduction of about 5% with respect to the previous *CR*, confirming that the sharper streamflow posterior uncertainty obtained through the multi-objective approach does not imply any significant drop in simulation reliability.

Table 3
Sharpness statistics for mean areal SWE over the period 01/10/2014 – 30/09/2017.

Sharpness	Min	Max	Mean	1th quartile	3th quartile
SWE (Meran/Merano)	0.13	0.45	0.32	0.26	0.39
SWE (Pfelders/Plan)	0.15	0.41	0.30	0.25	0.35

Table 4
Sharpness statistics for streamflow computed during the period 2014/10/01 – 2017/09/30 at Meran/Merano and Pfelders/Plan gauge stations. Sharpness statistics evaluated only over periods when the streamflow observations are included in the predictive uncertainty band are marked with label CR = 1.

Sharpness	Min	Max	Mean	1th quartile	3th quartile
Streamflow (Meran/Merano)	−0.14	0.50	0.11	0.01	0.19
Streamflow (Pfelders/Plan)	−0.09	0.64	0.17	0.06	0.28
Streamflow (Meran/Merano) – CR = 1	−0.11	0.47	0.13	0.05	0.20
Streamflow (Pfelders/Plan) – CR = 1	−0.09	0.64	0.17	0.06	0.27

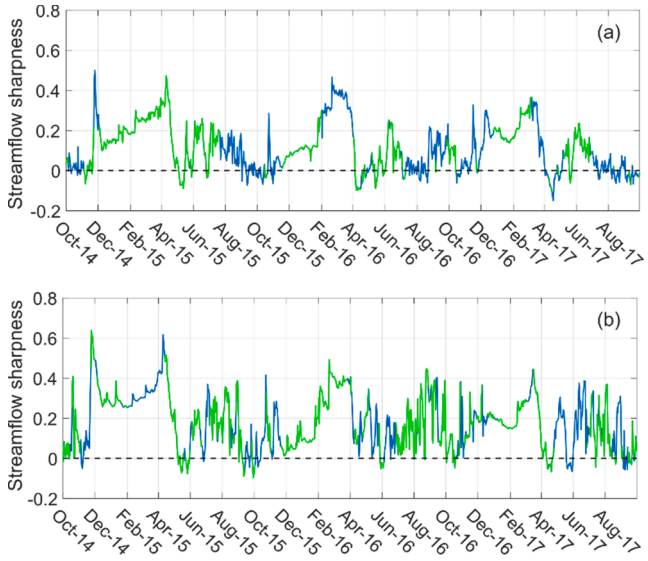

Fig. 6. Daily sharpness time series of streamflow at Meran/Merano (a) and Pfelders/Plan (b) gauging stations. The green lines represent days when the posterior uncertainty range includes the observed streamflow. (For interpretation of the references to colour in this figure legend, the reader is referred to the web version of this article.)

4. Discussion

4.1. Identification of thresholds for defining behavioural simulations

Likelihood measures and their associated thresholds used to identify behavioural simulations are a subjective choice of the modeller (Teweldebrhan et al., 2018; Shafii et al., 2014; Franks et al., 1998). As reported in Sect. 2, we used Nash-Sutcliffe efficiency index for both streamflow and *fSCA* variables. While NSE is an efficiency metric typically used in hydrology to evaluate the goodness of fit between simulated and observed streamflow, the same consideration does not hold for *fSCA* products. Indeed, most of the studies adopted Root Mean Square Error (*RMSE*) as objective function when dealing with snow cover area (see e.g., Duethmann et al., 2014; Notarnicola et al., 2013b; Parajka and Blöschl, 2008b) even though NSE was already used as evaluation metric

Table 5
Containing ratio (CR) for prior and posterior streamflow uncertainty ranges estimated at Meran/Merano and Pfelders/Plan stations, respectively, over the period 2014/10/01 – 2017/09/30. CR estimated considering only time steps with positive sharpness is marked with SH > 0 (last row). Bold fonts highlight the NSE threshold used throughout the work.

Containing ratio (CR)	Hydrometric station: Meran/Merano			Hydrometric station: Pfelders/Plan		
	NSE > 0.4	**NSE > 0.5**	NSE > 0.6	NSE > 0.4	**NSE > 0.5**	NSE > 0.6
Prior uncertainty range	0.55	**0.54**	0.53	0.77	**0.73**	0.68
Posterior uncertainty. range	0.56	**0.54**	0.54	0.71	**0.65**	0.60
Posterior uncertainty. range (SH > 0)	0.44	**0.46**	0.44	0.61	**0.59**	0.51

for *fSCA* (Udnæs et al., 2007; Pellicciotti et al., 2012). In the present work, we tested a three different objective functions to estimate *fSCA* likelihood, namely: NSE, RMSE and Klinge-Gupta efficiency index (KGE, Gupta et al., 2009). Among these three metrics, we found NSE as the best likelihood for updating the prior distribution, since it has shown relatively higher variability in the range of simulated efficiencies with respect to *RMSE* and KGE (results not shown for the sake of brevity). In this sense, NSE(*fSCA*) was more effective for a better identification of the combined posterior likelihood (see Eqn. (4)). We are aware that NSE index may overrate modelling performance of seasonal time series, such as *fSCA* (see e.g. Gupta et al., 2009), however in this study we are not interested in evaluating TOPMELT skills, already proven by other studies (Di Marco et al., 2020; Zaramella et al., 2019). Our aim is rather to select a likelihood measure for *fSCA* leading to the best possible identification of the posterior likelihood. NSE(*fSCA*) fits this purpose better than any other likelihood functions tested. Concerning the threshold values, we opted for the median of simulated NSE(*fSCA*) after several tests. Despite the range of variability of simulated NSE(*fSCA*) was larger than either *RMSE* and *KGE* cases, such range was still relatively narrow (NSE(*fSCA*) standard deviation equal to 0.125). Thus, the identification of a large threshold value would have made useless the estimation of the posterior likelihood (i.e., only few retained runs); on the contrary a small threshold value would have led to a poor identification of the posterior, and as a consequence to a negligible reduction of streamflow predictive uncertainty. Moreover, no existing guidelines on how to select *fSCA* threshold are proposed in literature, to the best of our knowledge. However, it should be noted that defining a likelihood threshold to identify acceptable models based on the distribution of such likelihood (i.e. the median likelihood) was recently prosed (Massmann, 2020). In that work, the authors compare multiple hydrological models in terms of streamflow simulation with a specific likelihood threshold set in order to retain behaviorals of every model, regardless the absolute value of such likelihood threshold.

The threshold value for streamflow was fixed equal to NSE*(Q)* = 0.5 (Fig. 3), according to Moriasi et al., (2007) to select acceptable model performance. However, we also tested the sensitivity of the results to NSE*(Q)* threshold by investigating the additional cases of NSE*(Q)* = 0.4 and NSE*(Q)* = 0.6. Table 5 shows the *CR* values using different NSE*(Q)* thresholds at both Meran/Merano and Pfelders/Plan sub-catchments. The lower the NSE*(Q)* threshold the higher the *CR* as a consequence of the increased number of retained behavioural simulations increases, which in turn leads to a larger prediction uncertainty band for streamflow at both locations. However, we notice how changing NSE*(Q)* threshold does not affect significantly the magnitude of *CR* variations at both locations (see Table 6). This result is in accordance with other studies showing that a small variation in the threshold value did not lead to significantly different uncertainty bounds prediction (Shafii et al., 2014; Lamb et al., 1998).

We remark that the Pareto plot shown in Fig. 3 is seldom reported in the literature despite the valuable information it provides, i.e. MODIS *fSCA* might be a very good additional data to be used in a multi-objective framework to reduce equifinality issue because of the very positive feedback with streamflow. To the author's knowledge only (Duethmann et al., 2014) plotted the likelihoods of *fSCA* and streamflow resulting from a Montecarlo-based procedure. We believe this is mostly related to the potentially unaffordable computational costs related to the simulation of the *fSCA* ensemble required. This need is hardly met by physically-based snow models and not surprisingly (Duethmann et al., 2014) used a temperature index approach for snowmelt modelling.

The snow model exploited in this work, TOPMELT, was conceived to balancing model structure complexity (i.e. it is more detailed than a degree-day model) and computational requirements. Thus, it represents an ideal tool to perform computationally intensive modelling. Accordingly, TOPMELT was already successfully applied in Montecarlo-like framework to quantify predicted *fSCA* uncertainty (Di Marco et al., 2020).

4.2. Improved model identifiability using multi-objective conditioning

Pareto fronts reported in Fig. 3 show a clear positive feedback between streamflow and *fSCA* simulations, suggesting that satellite-derived *fSCA* maps are a suitable product to inform the hydrological model. This agrees with previous findings using both MODIS and AVHRR retrievals (Finger et al., 2015; Duethmann et al., 2014; Roy et al., 2010; Parajka and Blöschl, 2008b). However, only Duethmann et al., 2014 reported a Pareto front between *fSCA* and streamflow, concluding that a good performance in terms of *fSCA* does not preclude a good simulation of discharge.

Moreover, such positive feedback indicates that the model conceptualization adopted allows a consistent simulation of both the response variables, see e .g., Piccolroaz et al., 2015. Different approaches for exploiting satellite-derived SCA maps are present in the literature, where simulated and observed SCA are compared either at the level of the individual elevation band (Duethmann et al., 2014; Parajka and Blöschl, 2008b) or even at pixel scale (Roy et al., 2010; Shrestha et al., 2014). In this work we rely on a simpler approach, considering the fraction of snow cover area to the total drainage basin, which has been already proven to be effective in the context of a multi-objective calibration (Teweldebrhan et al., 2018; Finger et al., 2015). Multi-objective conditioning based on the use of whole SCA map information might be addressed in future works, for instance to correct snowfall distribution at catchment scale, as suggested by Shrestha et al., (2014). However, in this paper our main goal is to assess the potential of combining MODIS SCA maps and streamflow records to better quantify model predictive uncertainty for gauged basins and for ungauged basins where parameter distributions are transposed from gauged basins. This might be especially useful at ungauged sites, thus providing the ground for a relatively easy way to implement a suitable framework for operational uses, e.g., in the context of short-term streamflow forecasting for hydropower exploitation.

Concerning the parameter identifiability, Fig. 4 depicts the comparison between prior and posterior snow-related parameter distributions. A clear improved identifiability of the Combined Melt Factor (*CMF*) parameter is obtained by constraining the model parameters with the additional MODIS *fSCA* data (Fig. 4a), while the other parameters do not show the same appreciable variation. We attribute this latter observation to the use of an aggregated efficiency metric, the fractional SCA, to condition the hydrological model. Using more accurate indexes, such as accounting for different elevation bands (Parajka and Blöschl, 2008b), might have led to a better parameter identifiability for the other

parameters of TOPMELT module, e.g. rainfall/snowfall threshold temperature T_c or fresh snow albedo. However accounting for different elevation bands to evaluate model performance is not straightforward, as pointed out by (Duethmann et al., 2014). Furthermore, developing an even more sophisticated pixel-based evaluation criterion would have implied to store the overall SCA maps instead of one scalar number (i.e. the *fSCA*), leading to computational constrain which would have limited the number of Monte Carlo simulation within the GLUE procedure.

The posterior distribution of *CMF* is more positively skewed than the prior one, with a peak around 0.018 mm m^2 $MJ^{-1}m^{-2}h^{-1}$. Larger *CMF* values are penalized in the posterior distribution likely because they would have led to unphysically fast snowmelt. Therefore, runs with larger *CMF* are associated with smaller values of the combined likelihood and they fall in the tails of the empirical cumulative likelihood weighted posterior distribution. In terms of predictive uncertainty range reduction this effect is evident by looking at the *fSCA* and streamflow time series relative to spring/summer 2015 (Fig. 5a1, Fig. 5b1 and Fig. 5c1), the year it snowed the most within the considered dataset (see Fig. 2a).

Visual inspection of streamflow predictive uncertainty bounds (i.e., 5–95% percentiles range) reveals that the reduction in the uncertainty band mostly occur during periods with high streamflow in spring and low streamflow in summer. Concerning spring, the better identifiability of the *CMF* parameter due to the multi-objective approach reduces the spring streamflow uncertainty mainly by preventing early snow melt due to high *CMF* values. Accordingly, the reduced low summer streamflow uncertainty is associated with high *CMF* values, because a decrease of summer runoff is related to an enhanced reduction of the accumulated snow mantle during spring. Concerning *fSCA*, the posterior distribution is sharper and more reliable compared with the prior one. Simulated *fSCA* tends to underestimate MODIS-based *fSCA* on late June, however satellite-derived estimates of SCA at the end of the melting season are known to be less accurate mainly because of cloud/snow misclassification (Notarnicola et al., 2013b) and dirty, patchy snowpack (Parajka and Blöschl, 2008a; Rittger et al., 2013) hamper an optimal snow detection by MODIS leading to a general overestimation of the actual SCA.

Fig. 6 shows the sharpness time series estimated at Meran/Merano and Pfelders/Plan gauging stations. The green line highlights the periods when *SH* is>0 as well as the posterior uncertainty band includes the observation. Here we focus our attention on Meran/Merano location since that was the gauging station adopted for constraining model parameters. During most of the investigated time period, *SH* is>0 (with an average value of 0.11), thus indicating that predictive uncertainty ranges of the posterior distribution is narrower than the prior. When *SH* is>0 the *CR* at Meran/Merano is 0.46 (Table 5), slightly lower than the *CR* value provided by the posterior and prior distributions throughout the whole period (both *CR* equal to 0.54). This proves that the uncertainty estimation adding MODIS *fSCA* is sharper than that performed using solely streamflow and it is still reliable, since the *CR* does not show a significant drop related to the shrink of the uncertainty streamflow band. Nonetheless, through the simulated period (mostly during April and the end of summer) a negative sharpness occasionally occurs, meaning that the posterior uncertainty range is wider than the prior and therefore no shrink of the predictive uncertainty occurs. This might be related to the aggregated metric used, i.e. the fractional snow cover area, which in some periods may not be completely informative. Indeed, besides *fSCA* also ground-based snow measurements might be used to inform hydrological models and reducing their uncertainty. However, point-scale snow depth observations have limited spatial representativeness (Scipión et al., 2013; Thirel et al., 2013; Grünewald et al., 2010) making challenging their use to represent snow dynamics at the catchment scale, unless a dense station network is present. However, some periods with negative sharpness are somehow expected when dealing with multi-objective framework, as reported by Efstratiadis and Koutsoyiannis, (2010) within its review paper on multi-objective approaches.

Finally, we estimated the predictive uncertainty for another variable, i.e. the mean areal snow water equivalent (SWE). Fig. 7a shows the predictive uncertainty of the mean areal SWE of the whole catchment closed at Meran/Merano gauging station. The shrinking of the uncertainty band is in this case evident and occurs throughout all the period of investigation, with an average sharpness value of 0.32 (Table 3). Reliability was not estimated since scarce SWE records are available, but it is still worth noting the potential of using MODIS *fSCA* data to obtain sharper uncertainty predictions of SWE, a key state variable for water resource strategy planning, e.g. for seasonal hydroelectric reservoir management, not often taking into account in uncertainty estimation analysis (Jobst et al., 2018).

4.3. Validation of uncertainty estimation procedure at internal sites

Model conditioning was performed using streamflow recorded at the Meran/Merano outlet section combined with MODIS-based *fSCA*. Those data are representative of the dynamics of the whole catchment, therefore evaluating reliability and sharpness of the uncertainty prediction at upstream nested sub-catchments can represent a valuable way to validate the robustness of the proposed approach since sub-catchment streamflow data were not involved in the parameter estimation procedure. Available data at Pfelders/Plan gauging station perfectly fit this objective.

Fig. 6b shows the daily streamflow sharpness estimated at Pfelders/Plan. Sharpness is>0 for most of the simulation time, thus supporting the idea that the addition of MODIS *fSCA* data can reduce the predictive streamflow uncertainty also at locations different from that used in the conditioning procedure. Overall, the mean *SH* value at Pfelders/Plan is 0.17 (Table 4), slightly greater than the value obtained at Meran/Merano (*SH* = 0.11).

On average, the reduction of the streamflow uncertainty is relatively small, yet not negligible since it can rise to 0.50 at Meran/Merano and 0.64 at Pfelders/Plan (Table 4). The uncertainty reduction found at Pfelders/Plan does not lead to a significant drop in simulated streamflow reliability, as proven by the CR statistics for Pfelders/Plan reported in Table 5. In the case of prior distribution CR is equal to 0.73, while it decreases only down to 0.65 when considering the posterior distribution. In particular, when only the period with positive sharpness is considered, *CR* equals 0.59. Therefore, *CR* values demonstrate a

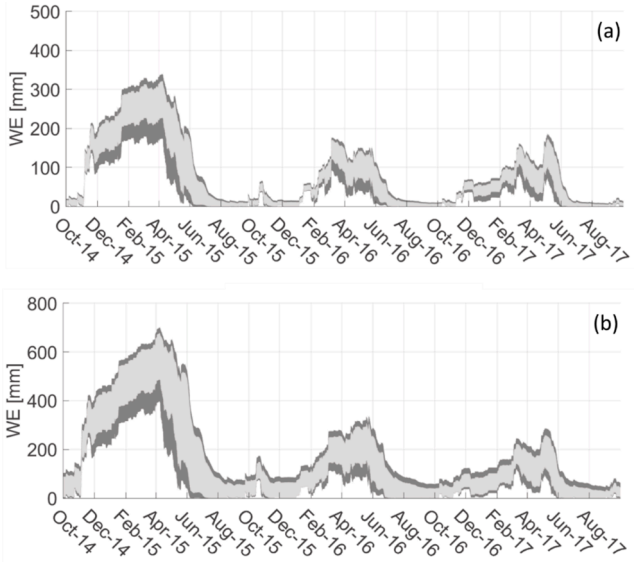

Fig. 7. Mean areal snow water equivalent (SWE) predictive uncertainty bounds at Meran/Merano (a) and Pfelders/Plan sub-basin (b). The dark grey area represents the prior while the light grey area represents the posterior distribution.

reasonably good capability of the model to reproduce streamflow at Pfelders/Plan location, which data we remind were not involved in the model conditioning. The slightly larger sharpness and *CR* with respect to Meran/Merano station case suggest that MODIS-related SCA maps are more informative at Pfelders/Plan, because snow dynamics plays a major role in this sub-catchment due to its higher altitude. Seasonal peak of SWE is indeed higher over the basin closed at Pfelders/Plan than for the Meran/Merano basin throughout the whole simulation period (Fig. 7). Moreover, Fig. 2 shows the monthly observed median flow at Meran/Merano and Pfelders/Plan hydrometric stations. The latter one displays a larger difference between winter low-flows and spring high-flows, suggesting therefore a larger contribution of snowmelt runoff in shaping the hydrograph, according to Schaefli et al., 2013.

To the best of our knowledge this is the first work presenting a spatial validation for a multi-objective uncertainty assessment, showing that better results are obtained at the validation site of Pfelders/Plan, rather than at the calibration site of Meran/Merano. This finding suggests that the proposed procedure may be more effective with increasing the altitude of concerned catchment.

Finally, we also investigated the predictive uncertainty bounds of SWE, a key variable to plan seasonal management of hydropower reservoirs in the region, yet not estimated together with streamflow in uncertainty analysis. Fig. 7 reports a comparison between the simulated time series of the mean areal SWE over Pfelders/Plan and Meran/Merano sub-catchments. At Pfelders/Plan, the average sharpness is 0.30, similar to the value estimated at Meran/Merano ($SH = 0.32$), thus supporting our idea that the multi-objective approach using MODIS-related products shows a good potential in inferring predictive SWE uncertainty reduction across the catchment. No reliability analysis was performed due to lack of measurements.

5. Conclusions

With this work we aim to evaluate a multi-objective parameter estimation framework which exploits MODIS-based snow cover maps to reduce predictive streamflow uncertainty in snow-dominated catchments. We performed this analysis over an Alpine catchment equipped with two hydrometric stations: one at the outlet of the main basin (Meran/Merano) and one internal, located upstream (Pfelders/Plan). The streamflow recorded at the outlet section was used to constrain the model parameters in order to build the prior distribution. Then, the posterior parameter distribution was obtained by using a multi-objective conditioning, i.e. by exploiting the MODIS-based fractional snow covered area (*fSCA*) as additional data. Streamflow data observed at the upstream internal station were used to spatially validate the model conditioning carried out using the overall catchment data (i.e. streamflow and satellite-based *fSCA* for the parent main basin).

Applying the GLUE framework with the joint use of streamflow and *fSCA* data arises computational issues, mainly because a large ensemble of *fSCA* is required. TOPMELT snow model fits perfectly this need thank to its parsimonious approach as well as its capability of simulating the snow water equivalent spatial distribution and, in turn, SCA.

Results showed that using MODIS-based *fSCA* to further condition the model parameters enhances the parameters identifiability, especially in the case of the Combined Melt Factor (*CMF*) and this in turn leads to a reliable and generally sharper uncertainty prediction of the streamflow with respect to the case in which only streamflow observations are used.

Sharper predicted uncertainty ranges for streamflow was found at the upstream Pfelders/Plan hydrometric station with respect to Meran/Merano, suggesting a promising application of the current multi-objective approach whenever it is of interest to infer the streamflow uncertainty range at ungauged locations.

Moreover, we investigated the predictive uncertainty band of the mean areal SWE. SCA maps proved themselves to provide valuable information to reduce significantly the predicted SWE uncertainty range at both Meran/Merano and Pfelders/Plan sites. The reliability of such sharper prediction was not assessed since only few direct SWE observations were available.

Finally, the described procedure can be easily extended to other catchments and it is not model dependent, i.e. any hydrological model able to estimate the fractional snow cover area can be in principle used. An extended temperature index model would be ideal due the balance between model complexity and computational efficiency.

Further work might concern the exploitation of the overall spatial information of the snow cover maps, rather than the aggregated fractional snow cover, perhaps considering also Sentinel or Landsat products along with MODIS. Introducing snow ground measurements to constrain snow-related model parameters might lead to a better parameter identifiability as well.

CRediT authorship contribution statement

Nicola Di Marco: Methodology, Software, Formal analysis, Investigation, Data curation, Writing - original draft. **Diego Avesani:** Validation, Data curation. **Maurizio Righetti:** Supervision, Project administration. **Mattia Zaramella:** Methodology, Investigation, Writing - review & editing. **Bruno Majone:** Conceptualization, Methodology, Supervision, Writing - review & editing. **Marco Borga:** Conceptualization, Methodology, Supervision, Writing - review & editing.

Declaration of Competing Interest

The authors declare that they have no known competing financial interests or personal relationships that could have appeared to influence the work reported in this paper.

Acknowledgments

Diego Avesani and Maurizio Righetti acknowledge the FESR1029 project, funded by the European Regional Development Fund (EFRE-FESR 2014-2020) and the Autonomous Province of Bolzano (Italy). Bruno Majone acknowledges support by the project "Seasonal Hydrological-Econometric forecasting for hydropower optimization (SHE)" funded within the Call for projects "Research Südtirol/Alto Adige" 2019 Autonomous Province of Bozen/Bolzano – South Tyrol, and by the Energy oriented Centre of Excellence (EoCoE-II), grant agreement number 824158, funded within the Horizon2020 framework of the European Union.

This work was supported by the Open Access Publishing Fund of the Free University of Bozen/Bolzano.

The Hydrographic Office of the Autonomous Province of Bolzano (http://meteo.provincia.bz.it) provided temperature, precipitation and streamflow data. We thank Claudia Notarnicola and Ludovica De Gregorio (EURAC, http://www.eurac.edu/it/research/mountains/remsen/) for providing MODIS snow cover maps as well as insightful suggestions about how to manage them. We thank the editor and two anonymous reviewers for their constructive comments, which helped us to improve the manuscript.

References

Avesani, D., Galletti, A., Piccolroaz, S., Bellin, A., Majone, B., 2021. A dual-layer MPI continuous large-scale hydrological model including Human Systems. Environ. Modell. Software 139, 105003. https://doi.org/10.1016/j.envsoft.2021.105003.

Bellin, A., Majone, B., Cainelli, O., Alberici, D., Villa, F., 2016. A continuous coupled hydrological and water resources management model. Environ. Modell. Software 75, 176–192. https://doi.org/10.1016/j.envsoft.2015.10.013.

Beven, K., 2006. A manifesto for the equifinality thesis. J. Hydrol. 320 (1–2), 18–36. https://doi.org/10.1016/j.jhydrol.2005.07.007.

Beven, K., Binley, A., 1992. The future of distributed models: Model calibration and uncertainty prediction. Hydrol. Process. 6 (3), 279–298. https://doi.org/10.1002/(ISSN)1099-108510.1002/hyp.v6:310.1002/hyp.3360060305.

Beven, K., Freer, J., 2001. Equifinality, data assimilation, and uncertainty estimation in mechanistic modelling of complex environmental systems using the GLUE methodology. J. Hydrol. 249 (1-4), 11–29.
Blasone, R.-S., Vrugt, J.A., Madsen, H., Rosbjerg, D., Robinson, B.A., Zyvoloski, G.A., 2008. Generalized likelihood uncertainty estimation (GLUE) using adaptive Markov Chain Monte Carlo sampling. Adv. Water Resour. 31 (4), 630–648. https://doi.org/10.1016/j.advwatres.2007.12.003.
Brazier, R.E., Beven, K.J., Freer, J., Rowan, J.S., 2000. Equifinality and uncertainty in physically based soil erosion models: application of the GLUE methodology to WEPP-the Water Erosion Prediction Project-for sites in the UK and USA. Earth Surf. Proc. Land. 25 (8), 825–845. https://doi.org/10.1002/1096-9837(200008)25:8<825::AID-ESP101>3.0.CO;2-3.
Brock, B.W., Willis, I.C., Sharp, M.J., 2000. Measurement and parameterization of albedo variations at Haut Glacier d'Arolla, Switzerland. J. Glaciol. 46 (155), 675–688. https://doi.org/10.3189/172756500781832675.
Chiogna, G., Majone, B., Cano Paoli, K., Diamantini, E., Stella, E., Mallucci, S., Lencioni, V., Zandonai, F., Bellin, A., 2016. A review of hydrological and chemical stressors in the Adige catchment and its ecological status. Sci. Total Environ. 540, 429–443. https://doi.org/10.1016/j.scitotenv.2015.06.149.
Di Marco, N., Righetti, M., Avesani, D., Zaramella, M., Notarnicola, C., Borga, M., 2020. Comparison of MODIS and Model-Derived Snow-Covered Areas: Impact of Land Use and Solar Illumination Conditions. Geosciences 10 (4), 134. https://doi.org/10.3390/geosciences10040134.
Duan, Q., Sorooshian, S., Gupta, V., 1992. Effective and efficient global optimization for conceptual rainfall-runoff models. Water Resour. Res. 28 (4), 1015–1031. https://doi.org/10.1029/91WR02985.
Duethmann, D., Peters, J., Blume, T., Vorogushyn, S., Güntner, A., 2014. The value of satellite-derived snow cover images for calibrating a hydrological model in snow-dominated catchments in Central Asia. Water Resour. Res. 50 (3), 2002–2021. https://doi.org/10.1002/2013WR014382.
Efstratiadis, A., Koutsoyiannis, D., 2010. One decade of multi-objective calibration approaches in hydrological modelling: a review. Hydrol. Sci. J. 55 (1), 58–78. https://doi.org/10.1080/02626660903526292.
Engel, M., Notarnicola, C., Endrizzi, S., Bertoldi, G., 2017. Snow model sensitivity analysis to understand spatial and temporal snow dynamics in a high-elevation catchment. Hydrol. Process. 31 (23), 4151–4168. https://doi.org/10.1002/hyp.v31.2310.1002/hyp.11314.
Finger, D., Vis, M., Huss, M., Seibert, J., 2015. The value of multiple data set calibration versus model complexity for improving the performance of hydrological models in mountain catchments. Water Resour. Res. 51 (4), 1939–1958. https://doi.org/10.1002/wrcr.v51.410.1002/2014WR015712.
Förster, K., Meon, G., Marke, T., Strasser, U., 2014. Effect of meteorological forcing and snow model complexity on hydrological simulations in the Sieber catchment (Harz Mountains, Germany). Hydrol. Earth Syst. Sci. 18 (11), 4703–4720. https://doi.org/10.5194/hess-18-4703-2014.
Franks, S.W., Gineste, P., Beven, K.J., Merot, P., 1998. On constraining the predictions of a distributed model: The incorporation of fuzzy estimates of saturated areas into the calibration process. Water Resour. Res. 34 (4), 787–797. https://doi.org/10.1029/97WR03041.
Gan, Y., Liang, X.-Z., Duan, Q., Ye, A., Di, Z., Hong, Y., Li, J., 2018. A systematic assessment and reduction of parametric uncertainties for a distributed hydrological model. J. Hydrol. 564, 697–711. https://doi.org/10.1016/j.jhydrol.2018.07.055.
Gascoin, S., Hagolle, O., Huc, M., Jarlan, L., Dejoux, J.-F., Szczypta, C., Marti, R., Sánchez, R., 2015. A snow cover climatology for the Pyrenees from MODIS snow products. Hydrol. Earth Syst. Sci. 19 (5), 2337–2351. https://doi.org/10.5194/hess-19-2337-2015.
Grünewald, T., Schirmer, M., Mott, R., Lehning, M., 2010. Spatial and temporal variability of snow depth and ablation rates in a small mountain catchment. The Cryosphere 4 (2), 215–225. https://doi.org/10.5194/tc-4-215-2010.
Gupta, H.V., Sorooshian, S., Yapo, P.O., 1998. Toward improved calibration of hydrologic models: Multiple and noncommensurable measures of information. Water Resour. Res. 34 (4), 751–763. https://doi.org/10.1029/97WR03495.
Gupta, H.V., Kling, H., Yilmaz, K.K., Martinez, G.F., 2009. Decomposition of the mean squared error and NSE performance criteria: Implications for improving hydrological modelling. J. Hydrol. 377 (1–2), 80–91. https://doi.org/10.1016/j.jhydrol.2009.08.003.
Jin, X., Xu, C.-Y., Zhang, Q., Singh, V.P., 2010. Parameter and modeling uncertainty simulated by GLUE and a formal Bayesian method for a conceptual hydrological model. J. Hydrol. 383 (3–4), 147–155. https://doi.org/10.1016/j.jhydrol.2009.12.028.
Jobst, A.M., Kingston, D.G., Cullen, N.J., Schmid, J., 2018. Intercomparison of different uncertainty sources in hydrological climate change projections for an alpine catchment (upper Clutha River, New Zealand). Hydrol. Earth Syst. Sci. 22 (6), 3125–3142. https://doi.org/10.5194/hess-22-3125-2018.
Laiti, L., Mallucci, S., Piccolroaz, S., Bellin, A., Zardi, D., Fiori, A., Nikulin, G., Majone, B., 2018. Testing the Hydrological Coherence of High-Resolution Gridded Precipitation and Temperature Data Sets. Water Resour. Res. 54 (3), 1999–2016. https://doi.org/10.1002/wrcr.v54.310.1002/2017WR021633.
Lamb, R., Beven, K., Myrabø, S., 1998. Use of spatially distributed water table observations to constrain uncertainty in a rainfall–runoff model. Adv. Water Resour. 22 (4), 305–317. https://doi.org/10.1016/S0309-1708(98)00020-7.
Madsen, H., 2003. Parameter estimation in distributed hydrological catchment modelling using automatic calibration with multiple objectives. Adv. Water Resour. 26 (2), 205–216. https://doi.org/10.1016/S0309-1708(02)00092-1.
Majone, B., Villa, F., Deidda, R., Bellin, A., 2016. Impact of climate change and water use policies on hydropower potential in the south-eastern Alpine region. Sci. Total Environ. 543, 965–980. https://doi.org/10.1016/j.scitotenv.2015.05.009.
Mallucci, S., Majone, B., Bellin, A., 2019. Detection and attribution of hydrological changes in a large Alpine river basin. J. Hydrol. 575, 1214–1229. https://doi.org/10.1016/j.jhydrol.2019.06.020.
Massmann, C., 2020. Identification of factors influencing hydrologic model performance using a top-down approach in a large number of U.S. catchments. Hydrol. Process. 34 (1), 4–20. https://doi.org/10.1002/hyp.v34.110.1002/hyp.13566.
Mazouz, R., Assani, A.A., Quessy, J.-F., Légaré, G., 2012. Comparison of the interannual variability of spring heavy floods characteristics of tributaries of the St. Lawrence River in Quebec (Canada). Adv. Water Resour. 35, 110–120. https://doi.org/10.1016/j.advwatres.2011.10.006.
McKay, M.D., Beckman, R.J., Conover, W.J., 1979. A Comparison of Three Methods for Selecting Values of Input Variables in the Analysis of Output from a Computer Code. Technometrics 21 (2), 239–245. https://doi.org/10.2307/1268522.
Moore, R.J., 1985. The probability-distributed principle and runoff production at point and basin scales. Hydrol. Sci. J. 30 (2), 273–297. https://doi.org/10.1080/02626668509490989.
Moore, R.J., 2007. The PDM rainfall-runoff model. Hydrol. Earth Syst. Sci. 11 (1), 483–499. https://doi.org/10.5194/hess-11-483-2007.
Moriasi, D.N., Arnold, J.G., Van Liew, M.W., Bingner, R.L., Harmel, R.D., Veith, T.L., 2007. Model Evaluation Guidelines for Systematic Quantification of Accuracy in Watershed Simulations. Trans. ASABE 50 (3), 885–900. https://doi.org/10.13031/2013.23153.
Nash, J.E., Sutcliffe, J.V., 1970. River flow forecasting through conceptual models part I — A discussion of principles. J. Hydrol. 10 (3), 282–290. https://doi.org/10.1016/0022-1694(70)90255-6.
Norbiato, D., Borga, M., Degli Esposti, S., Gaume, E. and Anquetin, S.: Flash flood warning based on rainfall thresholds and soil moisture conditions: An assessment for gauged and ungauged basins. Journal of Hydrology, 362(3–4), 274–290, doi: 10.1016/j.jhydrol.2008.08.023, 2008.
Norbiato, D., Borga, M., Merz, R., Blöschl, G., Carton, A., 2009. Controls on event runoff coefficients in the eastern Italian Alps. J. Hydrol. 375 (3–4), 312–325. https://doi.org/10.1016/j.jhydrol.2009.06.044.
Notarnicola, C., Duguay, M., Moelg, N., Schellenberger, T., Tetzlaff, A., Monsorno, R., Costa, A., Steurer, C., Zebisch, M., 2013a. Snow Cover Maps from MODIS Images at 250 m Resolution, Part 1: Algorithm Description. Remote Sensing 5 (1), 110–126. https://doi.org/10.3390/rs5010110.
Notarnicola, C., Duguay, M., Moelg, N., Schellenberger, T., Tetzlaff, A., Monsorno, R., Costa, A., Steurer, C., Zebisch, M., 2013b. Snow Cover Maps from MODIS Images at 250 m Resolution, Part 2: Validation. Remote Sensing 5 (4), 1568–1587. https://doi.org/10.3390/rs5041568.
Parajka, J., Bloschl, G., 2006. Validation of MODIS snow cover images over Austria. Hydrol. Earth Syst. Sci. 11.
Parajka, J. and Blöschl, G.: Spatio-temporal combination of MODIS images - potential for snow cover mapping. Water Resources Research, 44(3), doi:10.1029/2007WR006204, 2008a.
Parajka, J., Blöschl, G., 2008b. The value of MODIS snow cover data in validating and calibrating conceptual hydrologic models. J. Hydrol. 358 (3–4), 240–258. https://doi.org/10.1016/j.jhydrol.2008.06.006.
Parajka, J., Holko, L., Kostka, Z., Blöschl, G., 2012. MODIS snow cover mapping accuracy in a small mountain catchment - comparison between open and forest sites. Hydrol. Earth Syst. Sci. 16 (7), 2365–2377. https://doi.org/10.5194/hess-16-2365-2012.
Pellicciotti, F., Buergi, C., Immerzeel, W.W., Konz, M., Shrestha, A.B., 2012. Challenges and Uncertainties in Hydrological Modeling of Remote Hindu Kush–Karakoram–Himalayan (HKH) Basins: Suggestions for Calibration Strategies. Mt. Res. Dev. 32 (1), 39–50. https://doi.org/10.1659/MRD-JOURNAL-D-11-00092.1.
Piccolroaz, S., Majone, B., Palmieri, F., Cassiani, G., Bellin, A., 2015. On the use of spatially distributed, time-lapse microgravity surveys to inform hydrological modelling. Water Resour. Res. 51 (9), 7270–7288. https://doi.org/10.1002/2015WR016994.
Puspitarini, H.D., François, B., Zaramella, M., Brown, C., Borga, M., 2020. The impact of glacier shrinkage on energy production from hydropower-solar complementarity in alpine river basins. Science of Total Environment. 719, 137488.
Riboust, P., Thirel, G., Moine, N.L., Ribstein, P., 2019. Revisiting a simple degree-day model for integrating satellite data: implementation of swe-sca hystereses. Journal of Hydrology and Hydromechanics 67 (1), 70–81. https://doi.org/10.2478/johh-2018-0004.
Rittger, K., Painter, T.H., Dozier, J., 2013. Assessment of methods for mapping snow cover from MODIS. Adv. Water Resour. 51, 367–380. https://doi.org/10.1016/j.advwatres.2012.03.002.
Roy, A., Royer, A., Turcotte, R., 2010. Improvement of springtime streamflow simulations in a boreal environment by incorporating snow-covered area derived from remote sensing data. J. Hydrol. 390 (1–2), 35–44. https://doi.org/10.1016/j.jhydrol.2010.06.027.
Schaefli, B., Rinaldo, A., Botter, G., 2013. Analytic probability distributions for snow-dominated streamflow. Water Resour. Res. 49 (5), 2701–2713. https://doi.org/10.1002/wrcr.20234.
Scipión, D.E., Mott, R., Lehning, M., Schneebeli, M., Berne, A., 2013. Seasonal small-scale spatial variability in alpine snowfall and snow accumulation. Water Resour. Res. 49 (3), 1446–1457. https://doi.org/10.1002/wrcr.20135.
Scorpio, V., Andreoli, A., Zaramella, M., Moritsch, S., Theule, J., Dell'Agnese, A., Muhar, S., Borga, M., Bertoldi, W., Comiti, F., 2020. Restoring a glacier-fed river:

Past and present morphodynamics of a degraded channel in the Italian Alps. Earth Surf. Proc. Land. 45 (12), 2804–2823.
Sene, K., 2010. Hydrometeorology: forecasting and applications. Springer, Dordrecht; London.
Shafii, M., Tolson, B., Matott, L.S., 2014. Uncertainty-based multi-criteria calibration of rainfall-runoff models: a comparative study. Stoch. Env. Res. Risk Assess. 28 (6), 1493–1510. https://doi.org/10.1007/s00477-014-0855-x.
Shrestha, M., Wang, L., Koike, T., Tsutsui, H., Xue, Y., & Hirabayashi, Y.: Correcting basin-scale snowfall in a mountainous basin using a distributed snowmelt model and remote-sensing data. Hydrology and Earth System Sciences, 18(2), 747-761. https://doi.org.cyber.usask.ca/10.5194/hess-18-747-2014, 2014.
Simic, A., Fernandes, R., Brown, R., Romanov, P., Park, W., 2004. Validation of vegetation, MODIS, and GOES+ SSM/I snow-cover products over Canada based on surface snow depth observations. Hydrol. Process. 18 (6), 1089–1104. https://doi.org/10.1002/(ISSN)1099-108510.1002/hyp.v18:610.1002/hyp.5509.
Stergiadi, M., Di Marco, N., Avesani, D., Righetti, M., Borga, M., 2020. Impact of Geology on Seasonal Hydrological Predictability in Alpine Regions by a Sensitivity Analysis Framework. Water 12, 2255. https://doi.org/10.3390/w12082255.
Stigter, E.E., Wanders, N., Saloranta, T.M., Shea, J.M., Bierkens, M.F.P., Immerzeel, W. W., 2017. Assimilation of snow cover and snow depth into a snow model to estimate snow water equivalent and snowmelt runoff in a Himalayan catchment. The Cryosphere 11 (4), 1647–1664. https://doi.org/10.5194/tc-11-1647-2017.
Teweldebrhan, A.T., Burkhart, J.F., Schuler, T.V., 2018. Parameter uncertainty analysis for an operational hydrological model using residual-based and limits of acceptability approaches. Hydrol. Earth Syst. Sci. 22 (9), 5021–5039. https://doi.org/10.5194/hess-22-5021-2018.
Thirel, G., Notarnicola, C., Kalas, M., Zebisch, M., Schellenberger, T., Tetzlaff, A., Duguay, M., Mölg, N., Burek, P., de Roo, A., 2012. Assessing the quality of a real-time Snow Cover Area product for hydrological applications. Remote Sens. Environ. 127, 271–287. https://doi.org/10.1016/j.rse.2012.09.006.
Thirel, G., Salamon, P., Burek, P., Kalas, M., 2013. Assimilation of MODIS Snow Cover Area Data in a Distributed Hydrological Model Using the Particle Filter. Remote Sensing 5 (11), 5825–5850. https://doi.org/10.3390/rs5115825.
Tuo, Y., Marcolini, G., Disse, M., Chiogna, G., 2018. A multi-objective approach to improve SWAT model calibration in alpine catchments. J. Hydrol. 559, 347–360. https://doi.org/10.1016/j.jhydrol.2018.02.055.
Udnæs, H.-C., Alfnes, E., Andreassen, L.M., 2007. Improving runoff modelling using satellite-derived snow covered area? Hydrol. Res. 38 (1), 21–32. https://doi.org/10.2166/nh.2007.032.
Valéry, A., Andréassian, V., Perrin, C., 2014. 'As simple as possible but not simpler': What is useful in a temperature-based snow-accounting routine? Part 2 – Sensitivity analysis of the Cemaneige snow accounting routine on 380 catchments. J. Hydrol. 517, 1176–1187. https://doi.org/10.1016/j.jhydrol.2014.04.058.
Wagener, T., Boyle, D.P., Lees, M.J., Wheater, H.S., Gupta, H.V., Sorooshian, S., 2001. A framework for development and application of hydrological models. Hydrol. Earth Syst. Sci. 5 (1), 13–26. https://doi.org/10.5194/hess-5-13-2001.
Wagner, T., Themeßl, M., Schüppel, A., Gobiet, A., Stigler, H. and Birk, S.: Impacts of climate change on stream flow and hydro power generation in the Alpine region. Environmental Earth Sciences, 76(1), doi:10.1007/s12665-016-6318-6, 2017.
Warscher, M., Strasser, U., Kraller, G., Marke, T., Franz, H., Kunstmann, H., 2013. Performance of complex snow cover descriptions in a distributed hydrological model system: A case study for the high Alpine terrain of the Berchtesgaden Alps: complex snow descriptions in a hydrological model. Water Resour. Res. 49 (5), 2619–2637. https://doi.org/10.1002/wrcr.20219.
Yapo, P.O., Gupta, H.V., Sorooshian, S., 1998. Multi-objective global optimization for hydrologic models. J. Hydrol. 204 (1–4), 83–97. https://doi.org/10.1016/S0022-1694(97)00107-8.
Zaramella, M., Borga, M., Zoccatelli, D. and Carturan, L.: TOPMELT 1.0: a topography-based distribution function approach to snowmelt simulation for hydrological modelling at basin scale. Geoscientific Model Development, 12(12), 5251–5265, doi: 10.5194/gmd-12-5251-2019, 2019.
Zhang, Z., Wagener, T., Reed, P. and Bhushan, R.: Reducing uncertainty in predictions in ungauged basins by combining hydrologic indices regionalization and multiobjective optimization. Water Resources Research, 44(12), doi:10.1029/2008WR006833, 2008.